Rock Mechanics 14, 209—233 (1982)

Rock Mechanics
Felsmechanik
Mécanique des Roches

Fracture Initiation and Stress Wave Diffraction at Cracked Interfaces in Layered Media I. Brittle/Brittle Transition

By

H. P. Rossmanith and W. L. Fourney

With 12 Figures

(Received October 12, 1981)

Summary

Fracture Initiation and Stress Wave Diffraction at Cracked Interfaces in Layered Media — I. Brittle/Brittle Transition. Stress wave scattering about the tips of stationary interface cracks at a brittle-brittle junction in a layered medium and the associated stress-wave induced fracture were investigated. Dynamic photoelasticity was employed to visualize the highly complex interaction process between stress waves and cracks. Methods of linear elastic fracture mechanics were used to analyze regions of high stress intensity as possible sources for crack initiation. The phenomenon of partial load transmission across closed crack walls and imperfect joints and its effect on fracture initiation was also studied.

List of Symbols

c_l	longitudinal wave velocity in a plate $\sqrt{E/\varrho\,(1-\nu^2)}$
c_s	shear wave velocity $\sqrt{\mu/\varrho}$
h	normal distance from explosion to interface
a	crack length
b	distance between tips of two adjacent cracks
f_σ	dynamic photoelastic-fringe constant
N	photoelastic fringe order
σ_1, σ_2	principal normal stresses
τ_m	maximum shear stress
$\sigma_x, \sigma_y, \sigma_{xy}$	stress components in cartesian coordinates
$\sigma_r, \sigma_\theta, \sigma_{r\theta}$	stress components in polar coordinates
$\varkappa$	$=\varrho c_1$ acoustic impedance for plates
E	Young's modulus
ϱ	density

0035-7448/82/0014/0209/$ 05.00

μ	shear modulus
ν	Poisson's ratio
α_p, α_s	angles of incidence of longitudinal and shear waves
β_r, β_s	angles of reflection of longitudinal and shear waves
γ_p, γ_s	angles of refraction of longitudinal and shear waves

Wave Notation

P	longitudinal wave
S	shear wave
R	Rayleigh-wave
V	von Schmidt wave (generated by grazing incidence of P-wave)

Subscripts

r	reflected wave
d	diffracted wave
f	refracted wave
no subscript	incident wave
I, II	upper and lower half plane
superscripts	indicate the cracks tips

Introduction

Wave propagation and wave induced fracture in a layered media is of importance in the area of seismology as well as in removal of natural resources by mining engineering and hence has been the subject of many analytical and experimental investigations. The phenomenon of wave-crack interaction plays a basic role in geothermal heat exploitation, oil shale retort formation and typical bench fragmentation blasting. When this fragmentation is done inefficiently in a quarry operation additional expense is incurred to the mine operator. This added expense is seen as lost time in handling oversize fragments, time required in secondary breakage, and more frequent repairs to the primary crushers. In an oil shale application incorrect fragmentation could result in unsuccessful retorting. Knowledge of stress wave interaction with layer interfaces would help one to optimize fragmentation and consequently reduce the cost in mining operations or increase success rate in retort formation.

Formations encountered at quarry sites and oil shale deposits form stacks of layered rock with bedding planes and sets of joints present. The use of chemical explosives to fragment the material for further processing or to extend the fracture network is widespread. Upon detonation of an explosive the wave pattern generated in layered media is extremely complicated where incident and reflected wave systems not only interact with running cracks but also with existing cracks, flaws, inclusions or other inhomogeneities within the formation. Depending on the nature of the waves the cracks may

accelerate or decelerate during the interaction phase, and in some situations crack branching my be induced.

Theoretical aspects of elastic wave propagation and the interaction of stress waves with the interface between two dissimilar solid media with the resulting generations of reflected, refracted, and diffracted waves are well established and have been summarized in texts by Kolsky [1], Ewing, Jardetsky and Press [2], Achenbach [3], Graff [4] and Miklowitz [5]. Other contributions by Cagniard [6], White [7], Muskat and Meres [8], Heelan [9], Schmitt et al. [10], and Brekhoviskikh [11] concentrate on geophysical aspects of the wave propagation problem. Reflection, transmission, refraction and diffraction of plane and cylindrical waves about a stationary as well as a moving crack have been studied theoretically by Chen and Sih [12]. Diffraction of elastic waves about interface cracks in dissimilar media was investigated in detail by Brock [13—14].

In spite of this enormous body of theoretical background literature, it is difficult to obtain quantitative information in terms of stress magnitudes for real wave pulses, and real layer geometries with differing acoustic impedances. Experimental work has concentrated on point by point observations on the surface of the body and has consisted in measuring arrival times and wave velocities. More recently, dynamic photoelastic methods have been employed to study wave and crack propagation. Photoelastic studies with direct application to seismology are covered in papers by Dally, Riley and their coworkers [15—18]. Dynamic photoelasticity in conjunction with fracture mechanics has been applied successfully to problem of fragmentation and controlled blasting by the photomechanics laboratory at the University of Maryland in cooperation with industry during the past decade [19—22]. Current research programs at Maryland involve the study of problems related to optimizing quarry blasting, oil shale exploitation, and fracture initiation mechanisms in gas well stimulation [23—25].

This paper describes the application of dynamic photoelasticity in conjunction with fracture mechanics to the study of wave propagation and deals in particular with the interactions of stress waves with stationary and moving cracks located at the interfaces of dissimilar layers. Fracture initiation due to the various wave types is considered and stress magnitudes and stress intensity factor determinations were made in some instances. The effect of partial crack closure and bond imperfections on delayed dynamic load transmission across crack walls was determined and fracture network development was studied in detail.

The present investigation consists of two parts. Part I deals with fracture initiation by stress wave diffraction at cracked interfaces where similar brittle layers are bonded together. Part II covers the dynamic aspects of the interaction of stress waves and cracks at imperfectly bonded interfaces between dissimilar layers. The two-dimensional layered models were an attempt at modeling rock blasting and fragmentation in jointed formations. Observation obtained from production quarry blasting and oil shale exploitation sites seem to support the mechanisms of initiation that have been identified with this type of model testing.

Experimental Procedure

Dynamic photoelasticity was utilized to study wave interaction with interface cracks at the junctions of similar and dissimilar layers. Photoelastic methods offer full-field visualization and yield overall characteristics and numerical data during the period of the dynamic process. Information is obtained concerning instantaneous wave front location, stress wave amplitude distributions, crack tip position and the stress intensification at crack tips.

Internal point-source loading was generated by detonating an 80 mg charge of pentaerythritol tetranitrate (PETN) by means of a few mg's of lead azide (PbN_6) used as a primary explosive. PETN is a very suitable explosive for dynamic loading of photoelastic models as it generates stress pulses of short rise time ($\approx 1\,\mu s$) and the mean pulse width is about $5\,\mu s$. The explosive was highly packed in a 6 mm diameter borehole and a specially designed pressure containment device prevented the combustion gas products from venting. The detonation was initiated by a 2 kV-DC voltage pulse.

Rock joints in limestone quarries range from open mud-filled cracks to very tightly bonded calcite joints with properties similar to the adjoining rock masses. In the particular series of tests to be described, the bonding agent used was a product sold under the trade name "M Bond 200". This product is marketed by Eastman Chemical Products, Inc., and contains cyanoacrylate ester which sets rapidly under a slight pressure. The adhesive was spread uniformly with a resulting bond that was a few thousands of an inch (0.076 mm) in thickness. The joint would be classed as meduim to strong and all models could usually be handled without separation occurring. Tests on the bond showed the tensile strength to be about 1000 psi (6.9 MPa) and that the shear strength exceeded that of the model material (Homalite 100). The bond in the models would be approaching the condition encountered in a limestone calcite bond as opposed to mud filled or a weakly bonded interface.

All models used in the study consisted of two layers where the top layer contained the explosive at a site 75 mm from the interface (Fig. 1). The layers were fabricated from large sheets of Homalite-100 9 mm thick. It is manufactured by SGL Industries, Wilmington, Delaware, and is a birefringent polymeric material whose fracture properties have been well characterized [5]. The fracture thoughness, K_{Ic}, is typically about 400 psi-in$^{1/2}$ which means that it is more brittle than most rock types. Homalite 100 does not exhibit slow stable crack growth as does rock [6, 7], but the two are considered to exhibit similar response characteristics at high crack velocities. Thus it is felt that the results obtained can be qualitatively applied to rock like materials since fully coupled boreholes normally result in high crack propagation velocities.

Model 1 contained a single crack of 50 mm length with its near crack tip A directly under the explosive site whereas model 2 contained two cracks of 50 mm length in a row separated by a bonded bridge of 25 mm in length.

A multiple spark gap camera (Cranz-Schardin type) was employed to record the dynamic photoelastic fringe patterns. The camera was triggered by the detonation of the explosive and the exposure of the first negative occurred after a selected delay period. The camera used provides 16 frames

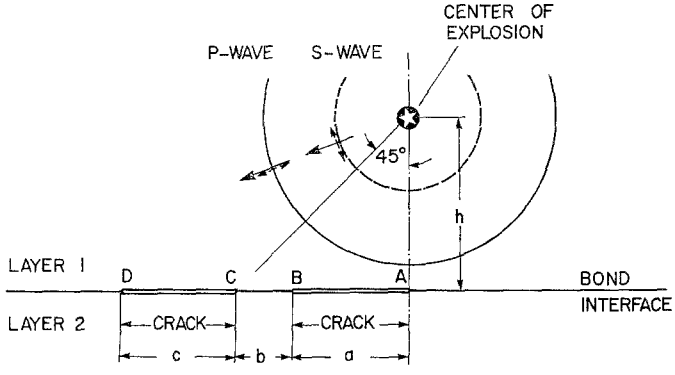

Fig. 1. Geometry and dynamic loading condition of cracked layer models. Diffraction of cylindrical *P*- and *S*-waves about the tips of a stationary double crack at a bonded interface
⟶ Direction of wave propagation; ⇢ direction of particle movement

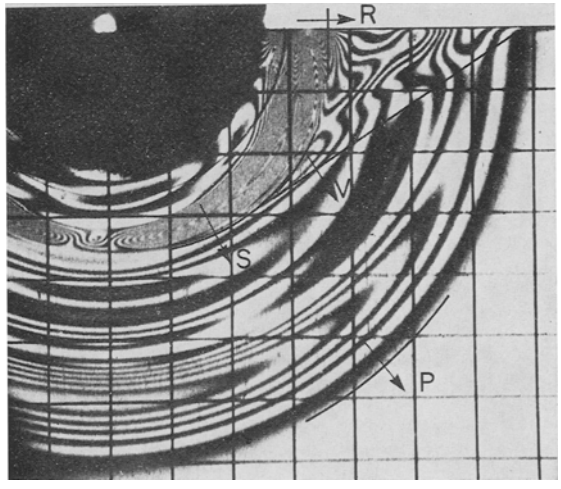

Fig. 2. Dynamic photoelastic recording of wave emission during explosive point force excitation at the free surface of a half-plane

at discrete times during the dynamic event. The sparks generate light pulses about 500 ns in duration and thus effectively stop the motion of the fringes during the exposure time. A framing rate of about 130,000 fps was used in these experiments. This provided an observation period of 100 μs after a delay time of some 40 μs which was well matched with the interaction process being studied.

A calibration test with an explosive detonating at the free boundary of a half plane provided the wave propagation velocities for Homalite 100: $c_l = 2100$ m/s, $c_S = 1200$ m/s, and $c_R = 1000$ m/s. The dynamic isochromatic recording of the calibration test is shown in Fig. 2 where the individual waves can be easily detected.

Theoretical Predictions

When elastic waves are generated and propagated during blasting or an earthquake phenomenon, they interact with geometric discontinuities or acoustical impedance mismatch zones and are reflected, refracted and diffracted and often give rise to a high elevation of local stresses. These stress concentrations become extremely severe when the discontinuity is a static or a moving crack. The result of waves reflecting and refracting about the crack tip may lead to unstable crack behavior and fracture initiation.

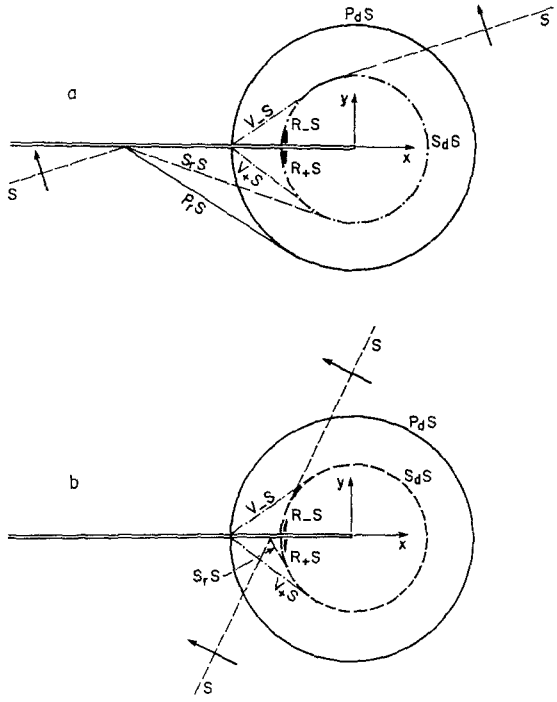

Fig. 3. Diffraction and reflection of a plane elastic longitudinal (*P*) Wave about a semi-infinite static crack, a) normal incidence, b) oblique incidence

The various waves which are generated during wave diffraction are well-established in theory. Upon detonation of the explosive a disturbance see e. g. Fig. 1 travels from the source outward through layer 1 as a cylindrical wave (*P*) at velocity c_l. It reaches the epoxy-bond interface at point A where it interacts with tip A of the crack $\overline{AB}$, giving rise to reflected and

diffracted waves. The energy carried by the incident P-wave is partitioned among the reflected and diffracted waves and the amplitude distribution along the wave fronts is very complex for both cylindrical and plane waves.

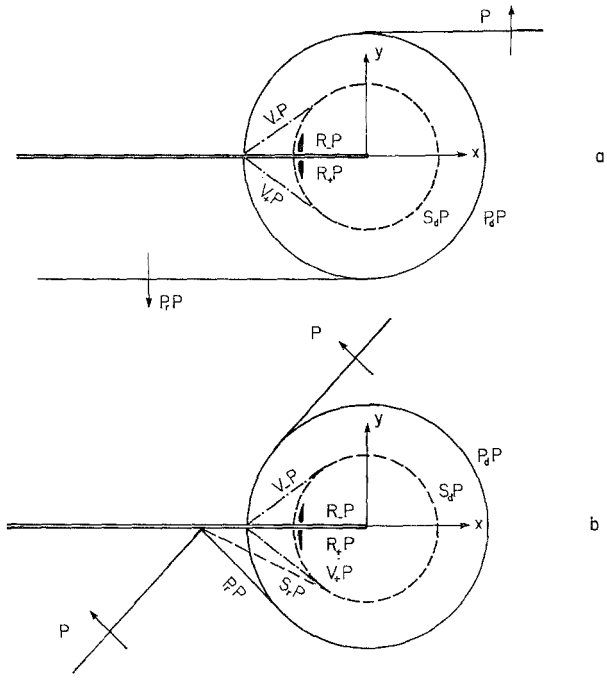

Fig. 4. Diffraction and reflection of an obliquely incident SV-wave about a stationary semi-infinite crack with angle of incidence (a) smaller and (b) larger than the angle of total reflection

If the stress at the crack tip is raised beyond a critical level cracks initiate from the interface and part of the energy carried by the incident wave is consumed by the propagating cracks. Explosive excitation of the borehole causes extensive crushing in the immediate vicinity around the hole which gives rise to a shear wave propagating at velocity c_S with cylindrical wave front.

The diffraction and reflection of a plane longitudinal (P) elastic wave about a semi-infinite static crack is shown in Fig. 3 for obliquely (b) and normally (c) incident wave fronts. Upon impingement of the initial P-wave front at an angle α_p (included angle between the normal to the wave front and the normal to the crack line) two diffracted waves, a longitudinal P_dP-wave and a rotational S_dP-wave originate at the site of the crack tip and propagate radially outward. Two reflected waves, P_rP and S_rP result from the reflection of the P-wave at the crack wall facing the incident wave pulse; the reflected shear wave S_rP, however, is absent for $\alpha_p = 0^0$. In addition, von Schmidt waves, V_+P and V_-P, are being generated by the grazing

incidence of the P_dP wave during its travel along the crack faces. These waves are shear waves which subtend an angle of $\sin^{-1}(c_s/c_l)$ with respect to the crack line.

When a shear wave S interacts with a crack tip the types of waves generated during the interaction process depend on the angle of incidence α_s of the shear wave. Figs. 4a and 4b illustrate two representative cases: (a) where α_s is smaller than a critical angle of incidence and, hence, two reflected waves, P_rS and S_rS, and two diffracted waves, P_dS and S_dS, are generated; and (b) where α_s is larger than the critical angle of total reflection where no P_rS-wave is generated. Similarly, the grazing incidence of the P_dS-wave gives rise to von Schmidt waves $V_{\pm}S$. In the general case where both, P- and S-waves impinge, $V_{\pm}S$ and $V_{\pm}P$ waves propagate along the faces of the crack after being generated by the grazing incidence of the diffracted P_dS- and P_dP-waves, respectively. It is to be noted that two-dimensional dynamic photoelasticity deals with in-plane deformations, and highlights longitudinal (P) waves and the component of a shear wave which is polarized parallel to the specimen plane which induces in-plane shear deformations (SV-waves). In geophysics, where the medium often is a half-space, SV-waves induce motion in a vertical plane, i. e. in a plane normal to the earth's surface and contains both vertical and horizontal components of motion, whereas SH-waves induce motion exclusively in planes parallel to the earth's surface.

The resulting stress field $\sigma_{ij}(x, y, t)$ associated with the wave-crack interaction process is composed of the stress field of the incident wave $\sigma_{ij}^{(i)}(x, y, t)$ and scattered wave field $\sigma_{ij}^{(s)}(x, y, t)$:

$$\sigma_{ij}(x, y; t) = \sigma_{ij}^{(i)}(x, y; t) + \sigma_{ij}^{(s)}(x, y; t) \tag{1}$$

where the scattered field must satisfy the radiation condition

$$\sigma_{ij}^{(s)} \to 0. \tag{2}$$

As a result of wave-crack interaction the following zones can be identified for an incident P-wave (Fig. 5a):

I — undisturbed region
II — incident pulse zone
III — shadow zone
IV — geometric reflection zone
V — dilatational wave scattering zone
VI — von Schmidt-wave zone
VII — shear wave scattering zone

Based on the theory of elastic wave propagation the following various stages of wave formation are predicted for the one-crack-model (see Fig. 1):

1. P-pre-interaction phase: $0 < t < h/c_l = 75$ mm/2100 m/s $= 36$ μs. This is the time delay between detonation of the explosive and arrival of the incident P-wave front at crack tip A.

2. Wave reflection phase: $h/c_l < t < \{h^2+a^2\}^{1/2}/c_l = 43\ \mu s$. In this interval, the incident cylindrical P-wave front has reached crack tip B. Two reflected waves P_rP and S_rP and two diffracted waves P_d^AP and S_d^AP are generated. Grazing incidence of the P_d^AP wave along the crack walls induces von Schmidt head waves V_+P and V_-P.

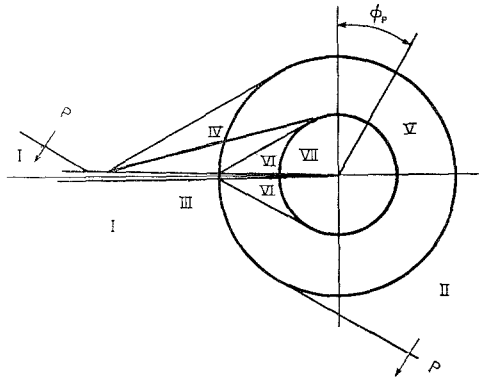

Fig. 5 a. Various regions associated with an obliquely incident P-wave scattered about a crack tip

3. S-pre-interaction phase: $0 < t < h/c_s = 75$ mm/1200 m/s $= 62.5\ \mu s$. This is the time span required for the shear wave generated due to fracturing and crushing the borehole wall to approach crack tip A.
4. Secondary diffraction at crack tip B starts at time $t = (h+a)/c_l = 60\ \mu s$ after detonation; whereas secondary diffraction at crack tip A starts at time $t = [(h^2+a^2)^{1/2}+a]/c_l = 67\ \mu s$.
5. Interaction of incident shear wave with scattered P-wave field: $t > \{h^2+a^2\}^{1/2}/c_s = 75\ \mu s$ for crack tip B and $t > 67\ \mu s$ for crack tip A.

During these interaction phases the transient wave stress fields superimpose and may produce stresses above the fracture stress of the material.

In fracture mechanics the deformation of the crack walls induced by the wave motions are classified in three modes: mode-1 → normal spacing mode deformation, mode-2 → in-plane shearing mode deformation, and mode-3 → anti-plane shearing mode deformation. The $r^{-1/2}$ stress singularity is retained for crack-wave interaction problems.

Because the total wave field contains both P- and SV-wave contributions a transient mixed-mode stress intensity factor $K = K_1 - iK_2$ is introduced in the general case [25]. The angular distribution of stress around a static crack tip during dynamic loading due to harmonic wave diffraction is the same as in the case of static loading except for the transient amplitude. Within the linear theory of elasticity a real pulse may be Fourier-analyzed and, hence, the static angular stress distribution applies also for single wave pulses which impinge upon a static crack.

The situation is more complex for wave diffraction with moving cracks. Here, the stress singularity is the same as that of stationary cracks while the angular variation of the stress field around the crack tip is increasingly distorted with increasing crack velocity. The dynamic stress intensity factors K_1 and K_2 for the moving-crack/wave interaction process are complicated functions of the circular frequency, the input wave amplitudes, angles of incidence, and crack speed [12].

Fracture Analysis

Separation of stresses based on photoelastic data is possible only under special circumstances, such as the case of polar loading symmetry [26]. An elastic analysis was used to separate stresses along a bond-line during the

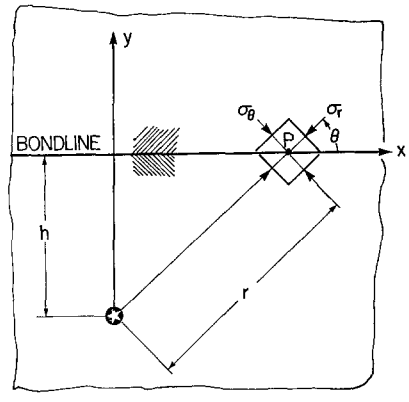

Fig. 5 b. State of stress in a material element located at the bondline during the passage of a longitudinal wave

passage of a cylindrical P-wave. The cartesian stress components σ_x, σ_y, and τ_{xy} at a location P (see Fig. 5b) with coordinates

$$x = \sqrt{r^2 - h^2}\,, \quad y = 0 \tag{3}$$
$$r, \theta = \tan^{-1}(h/x)$$

are most easily determined from the polar stress components by theory of elasticity

$$\sigma_x = (\sigma_r + \sigma_\theta)/2 + (\sigma_r - \sigma_\theta)/2 \cdot \cos 2\theta$$
$$\sigma_y = (\sigma_r + \sigma_\theta)/2 - (\sigma_r - \sigma_\theta)/2 \cdot \cos 2\theta$$
$$\tau_{xy} = (\sigma_r - \sigma_\theta)/2 \sin 2\theta. \tag{4}$$

The polar stress components σ_r and σ_θ which represent the principal normal stresses for a cylindrical symmetric loading must be determined from the information contained in the isochromatic fringe pattern. A simple separa-

tion technique which is particularly helpful in this study is based upon Hooke's law, the strain-displacement relations in polar coordinates, and the stress optic law of photoelasticity:

$$\varepsilon_\theta = -\frac{(1+\nu)}{E}\frac{f_\sigma}{D}\int_r^{r_0}\frac{N(r')}{r'}\,dr'$$
$$\varepsilon_r = \varepsilon_\theta - \frac{(1+\nu)}{E}\frac{f_\sigma}{D}N(r) \tag{5}$$

and

$$\sigma_\theta = \frac{E}{1-\nu^2}(\varepsilon_\theta + \nu\varepsilon_r)$$
$$\sigma_r = \frac{E}{1-\nu^2}(\varepsilon_r + \nu\varepsilon_\theta) \tag{6}$$

where E, ν, f_σ, and D are the Young's modulus, Poisson's ratio, material fringe value and model thickness, respectively, of a two-dimensional photoelastic specimen, $N(r)$ is the fringe value of the outgoing P-wave at radial position r, and r_0 is any value of the radial distance r ahead of the leading wavefront of the P-wave (reference radius). A Simpson procedure for unequally spaced data was used to evaluate the integral in Eqs. (5). Typical results for the separated stresses σ_r and σ_θ obtained by J. Philips [27] for a model that did not contain a bond line show that in the leading part of the P-wave both principal stresses are compressive with the radial stress σ_r about three to four times as large as the hoop stress σ_θ. On the trailing tensile half of the P-wave σ_θ is larger than σ_r and σ_r may actually never reach a tensile value.

Two fracture mechanisms have been observed in the course of these experiments: shear cracking initiated by the obliquely incident leading compressive part of the P-pulse and mixed-mode cracking as a result of the interaction of the trailing tensile part of the P-pulse possibly in conjunction with the leading shear wave front.

Shear Cracking of Perfectly Bonded Layers

For an increase in stress of the nature found in the compressive biaxial P wave one would expect the greatest values of τ_{xy} to occur for $\theta = 45^0$ (see Eqs. (4)). Typical mode-2 bond line cracking has been observed experimentally at these locations during the early time loading of bonded layers such as the example shown in Fig. 6a. This figure was taken from reference [30] and shows the stress state 53 μs after a detonation occurred in a multiple layered model with no intentional bond imperfections. Note that the fractures have initiated most heavily at the $\theta = \pm 45$ degree locations and extend only into the material not containing the charge. Notice also that the fractures are initiated ahead of the outgoing shear wave indicating that the P wave compressive peak is responsible for the nucleation and initiation.

Shear Cracking of Imperfectly Bonded Layers

Figs. 6b and 6c show a sequence of photographs taken in the present series of tests with a single interface crack $\overline{AB}$ (debond section) between the two layers. Here the situation is different than in Fig. 6a. The leading compressive part of the obliquely impinging *P*-wave gives rise to crack load-

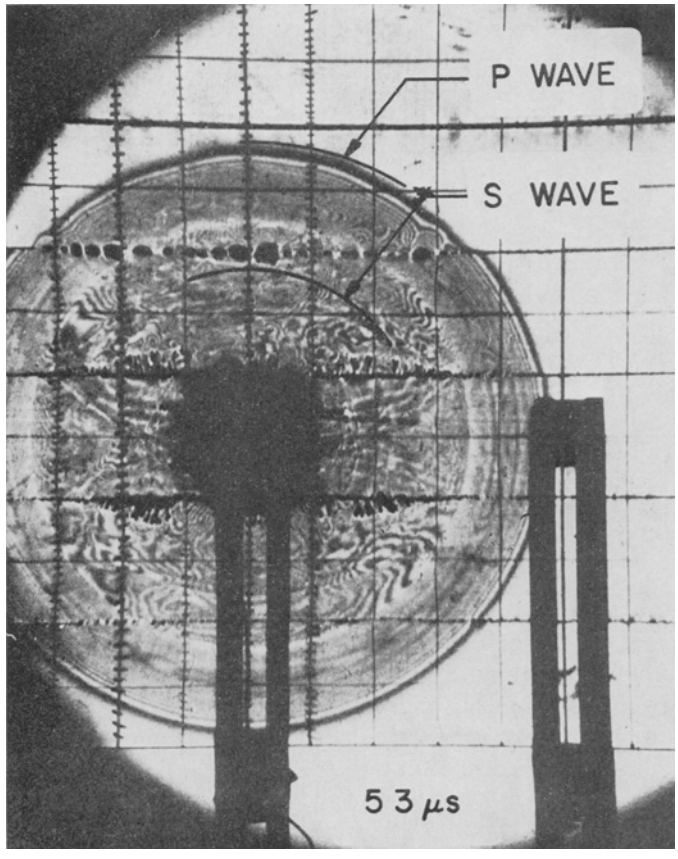

Fig. 6 a. Joint initiated cracks created from a perfect bond

ing by compression *and* shear. The state of stress in the neighborhood of a crack loaded in compression with the crack walls partially closed or separated by fillets is given by

$$\begin{aligned}
\sigma_x(\varrho,\phi) &= -\frac{K_2}{\sqrt{2\pi\varrho}}\sin\frac{\phi}{2}\left(2+\cos\frac{\phi}{2}\cos\frac{3\phi}{2}\right)\\
\sigma_y(\varrho,\phi) &= \frac{K_2}{\sqrt{2\pi\varrho}}\sin\frac{\phi}{2}\cos\frac{\phi}{2}\cos\frac{3\phi}{2}\\
\tau_{xy}(\varrho,\phi) &= \frac{K_2}{\sqrt{2\pi\varrho}}\cos\frac{\phi}{2}\left(1-\sin\frac{\phi}{2}\sin\frac{3\phi}{2}\right)
\end{aligned} \tag{7}$$

where ϱ and ϕ are coordinates of a polar system centered at the crack tip with the crack extending along $\psi = \pm\pi$. K_2 is the mode-2 stress intensity

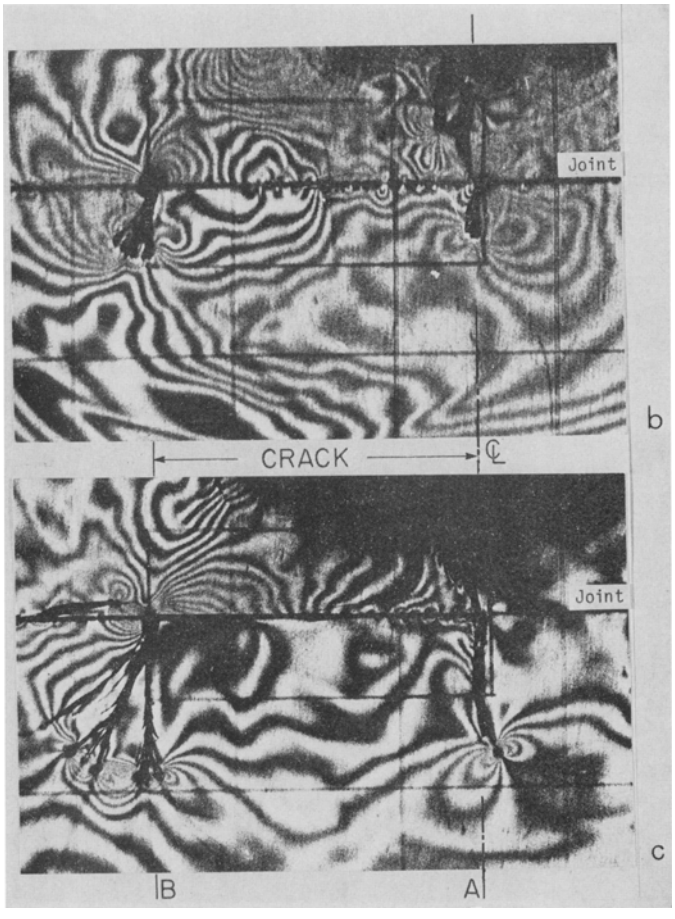

Fig. 6 b, c. Development of layer cracking from the crack tips at the bond interfarce Homalite 100 — Epoxy bond — Homalite 100
b) Initiation from the tips of an interface crack — early phase; c) later phase

factor which for a central crack of length 2a subjected to shear loading and exhibiting friction between the crack walls is given by

$$K_2 = (\tau_{xy} - \tau)\sqrt{\pi a} \tag{8}$$

with the friction stress

$$\tau_r = \mu\,|\sigma_y| \tag{9}$$

where μ is a modified coefficient of friction which takes into account the shear stiffness of the bond material.

Eqs. (7)—(9) hold with sufficient accuracy if the pre-existing bond-separation length 2a is small, i. e. when the stress components of the incoming P-wave do not considerably vary along the crack line.

Fracture initiation occurs when a certain critical condition is satisfied which could be achieved either by exceeding a critical fracture stress (as required by the maximum tensile stress criterion) or by exceeding some other critical quantity characteristic for fracture, e. g., the strain energy density. The principal stresses σ_1 and σ_2 are computed from the relations

$$\sigma_{1,2} = \frac{\sigma_x + \sigma_y}{2} \pm \sqrt{\left(\frac{\sigma_y - \sigma_x}{2}\right)^2 + \tau_{xy}^2} \tag{10}$$

and the orientation ω of the maximum principal normal stress with respect to the x-axis is given by

$$\omega(\phi) = \frac{1}{2} \tan^{-1}\left(\frac{2\tau_{xy}}{\sigma_y - \sigma_x}\right), \tag{11}$$

Fig. 7a shows the variation of the principal normal stresses σ_1 and σ_2, and the orientation ω in the range $-\pi < \phi < \pi$ for a mode-2 crack problem.

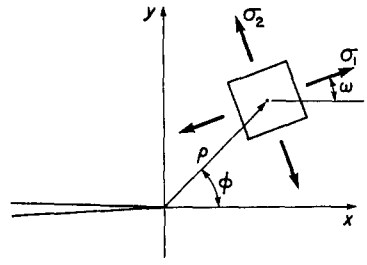

Fig. 7 a. Orientation of principal normal stresses for a mode two crack problem

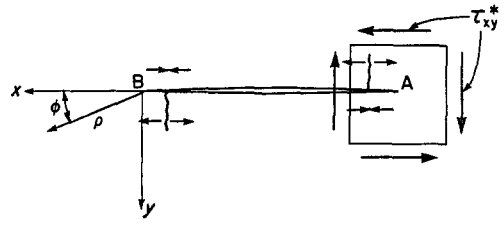

Fig. 7 b. Layer cracking produced by outgoing P-waves at interface crack tips

The shear stress at the bondline (τ_{xy}) is the only component of the stress field that introduces a singular stress distribution at the tip of the pre-existing interface crack when negative (compressive) stresses σ_x and σ_y occur.

For a positive far-field shear stress τ_{xy}^* (Fig. 7b), the shear stress associated with the outgoing P-wave, the stress σ_1 attains its maximum value for $\theta = -\pi$, i. e. along the lower face of the crack. For traction-free boundary condition along the crack edges eqn. (11) yields for the orientation $\omega = 0$ or $\pi/2$ as ϕ approaches $\pm\pi$. Because the resolved shear stress $\tau_{xy}^{(p)}$ along the bondline during the initial P-wave passage is negative, the maximum tensile stress is expected to occur at point A at the positive edge of the crack $\overline{AB}$

as depicted in Fig. 7b. Similarly crack initiation is expected to occur at point B on the negative side of the crack with the branch crack emerging normally to the interface crack into the lower layer. This is shown in Figs. 6b and 6c. The other crack at A propagating into the lower layer was generated as a result of the interaction of the outgoing *shear* wave with the crack not the P wave. This is supported by the fact that the crack in the lower layer at B is longer than the one at A and was more likely initiated earlier.

The crack initiation angle with respect to the crack line is 90 degrees when employing a maximum tensile stress criterion whereas it is 82.7^0 (for $\nu=0.31$) according to Sih's strain energy density criterion for pure mode-2 cracking. This shear cracking mechanism is depicted very clearly in Fig. 8b for crack AB in the two crack model. Notice in Fig. 8b at tip A the fracture initiates and travels upward towards the borehole with no extension into the lower layer, while at tip B its initiation and propagation direction is downward into the lower layer. Notice also in Fig. 8c taken 12 μs later that the shear wave has initiated a second crack at A which travels downward into the lower layer.

As the bond thickness decreases or the modulus of the layer material decreases the time required for partial or full crack closure decreases. With increasing contact of the rough crack walls the effective shear stress component in Eq. (8) is lowered by the frictional stress increase. This induces a lower value for K_2 and, hence, shear crack initiation as depicted in Figs. 6b, 6c and Fig. 8 may not occur. In the limit for a perfect bond the crack initiation mechanism is such that no cracks propagate into the borehole layer (Fig. 6a).

As was stated earlier the most extensive fracturing is to be expected in the region around crack tip B where the resolved shear stress is maximized, i. e. at an angle of 45^0 from the normal line through the borehole. This assumes that the stress amplitude of the outgoing cylindrical P-wave (which decays proportional to $r^{-1/2}$ with distance of travel) [27] is strong enough at the bondline to initiate fracture. It is interesting to note that a static analysis yields a much faster decay of a cylindrical stress field proportional to r^{-2}, and hence the result of a static analysis would be too conservative with respect to fracture initiation.

Mixed-mode Cracking

Oblique incident of the trailing tensile part of the P-wave gives rise to mixed-mode crack loading. The near tip stress field associated with combined opening and shearing mode crack deformation is given by

$$\sigma_x=\frac{K_1}{\sqrt{2\pi\varrho}}\cos\frac{\phi}{2}\left[1-\sin\frac{\phi}{2}\sin\frac{3\phi}{2}\right]-\frac{K_2}{\sqrt{2\pi\varrho}}\sin\frac{\phi}{2}\left[2+\cos\frac{\phi}{2}\cos\frac{3\phi}{2}\right]$$

$$\sigma_y=\frac{K_1}{\sqrt{2\pi\varrho}}\cos\frac{\phi}{2}\left[1+\sin\frac{\phi}{2}\sin\frac{3\phi}{2}\right]+\frac{K_2}{\sqrt{2\pi\varrho}}\sin\frac{\phi}{2}\cos\frac{\phi}{2}\cos\frac{3\phi}{2}$$

$$\tau_{xy}=\frac{K_1}{\sqrt{2\pi\varrho}}\sin\frac{\phi}{2}\cos\frac{\phi}{2}\cos\frac{3\phi}{2}+\frac{K_2}{\sqrt{2\pi\varrho}}\cos\frac{\phi}{2}\left[1-\sin\frac{\phi}{2}\sin\frac{3\phi}{2}\right].$$

Crack advancement due to mixed-mode conditions also occurs in a direction other than along the bondline.

Double-Crack at a Bondline

Fig. 8 shows the diffraction of a cylindrical *P*-wave about a double interface crack at the joint line of a Homalite 100 — Epoxy bond — Homalite 100 plate where the first crack extends from *A* to *B* and the second

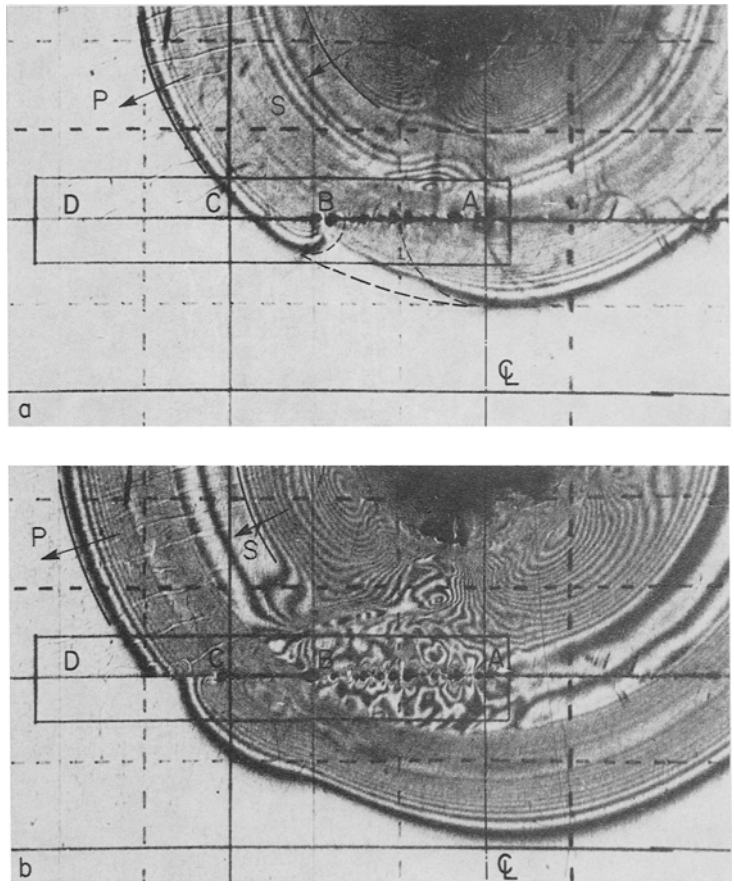

Fig. 8. Sequence of dynamic photoelastic fringe patterns showing *P*-wave diffraction about a double interface crack at a point Homalite 100 — Epoxy bond — Homalite 100 (first crack $\overline{AB}$, second crack $\overline{CD}$, Test LM-4)
a) Frame 3, $t=48\ \mu s$; b) frame 4, $t=58.5\ \mu s$

cracks extends from *C* to *D*. The geometry of the models is selected such that the outgoing *P*-wave impinges normally onto the crack line at Point *A* whereas the angle between the borehole radial passing through crack tip C of the second crack and the crack line is $\pi/4$.

Fig. 8a depicts the situation where the incident P-wave is already diffracted about the crack tips A and B. Theory predicts a quarter-circle shaped diffraction region in the lower layer at crack tip A and a similarly shaped diffraction region at crack tip B as indicated by two circular arcs in Fig. 8a. The undisturbed P-wave front if there was no crack present is also marked in the same figure. For an open interface crack where there is no crack face closure, the shadow region bounded by the broken lines and a section of the lower crack edge is stress free. Fig. 8a, however, shows that appreciable stress wave load transmission across the temporarily closed crack gap occurred. The delay time, i. e. the time necessary to bring the crack walls in contact to permit passage of the P-wave across the interface crack varies along the crack line. It increases with increasing angle of incidence of the P-wave and in this test an average value of about 4 μs was determined. In general the time for crack closure is a function of the thickness of the bond layer, the mechanical properties of the bond material as well as the layer materials and the angle of incidence of the impinging P-wave. The effect of the latter is shown in Fig. 8b in the vicinity of crack tip C. Apparently, the angle of incidence of the P-wave $\theta_p = 45^0$ is too large for the successful build-up of a normal pressure component of the P-wave stress to bring the two crack walls into contact. Hence no load is being transmitted across the crack walls and the theoretically predicted shape of the diffraction region is retained on the lower crack wall $\overline{CD}$.

Fracture Network Development from Multiple Bondline Cracks

The sequence of six dynamic photoelastic recording shown in Fig. 9 covers the wave interaction with bondline cracks and show bondline crack initiation and propagation. The enlargements show the section of the bondline where the double-interface-crack is located.

The first photograph, frame 6, shown in Fig. 9a, was taken 79.5 μs after the detonation of the borehole charge. The P-wave front has already passed the site of crack tip D whereas the peak of the leading compressive P-wave pulse showing a visible fringe order $N_{max} = 8$ is in full interaction with crack tip D. The local irregularity in the wave front reveals a minor bond imperfection to the left of crack tip D and it shows that no load was transmitted across the second crack. Layer cracking starts from crack tips A, B, and also C. It is convenient to define a unit normal to a crack tip in the direction of the crack line as sketched schematically in Fig. 10. Then, frames 6 to 9 (Figs. 9a to 9c) reveal that layer cracking starts from a bondline crack in a direction which makes an angle of slightly less than 90^0 clockwise with respect to the crack tip unit normal. This follows from the analysis in the preceding sections. Local P_rP- and S_rP-waves generated by reflection of the incident P-wave along the upper crack wall extending between crack tips C and D and moving towards the upper left corner are clearly distinguishable in Figs. 9a to 9c. Although not clearly distinguishable these wave fronts merge with diffracted waves $P_d^C P$ and $S_d^C P$, and

$P_d^D P$ and $S_d^D P$ radiating from the crack tips C and D, respectively. Incipient layer fracturing is visible at point D in frame 7, Fig. 9b.

The radial outwardly propagating borehole fractures are outdistanced by the high-intensity shear wave, a portion of which is clearly visible in Fig. 9b between points B and C. The structure of the shear wave is extremely complicated. Upon detonation of the explosive a system of radial cracks which originate at arbitrary locations around the rough borehole wall propagate radially outward. This destroys the initially existing cylindrical

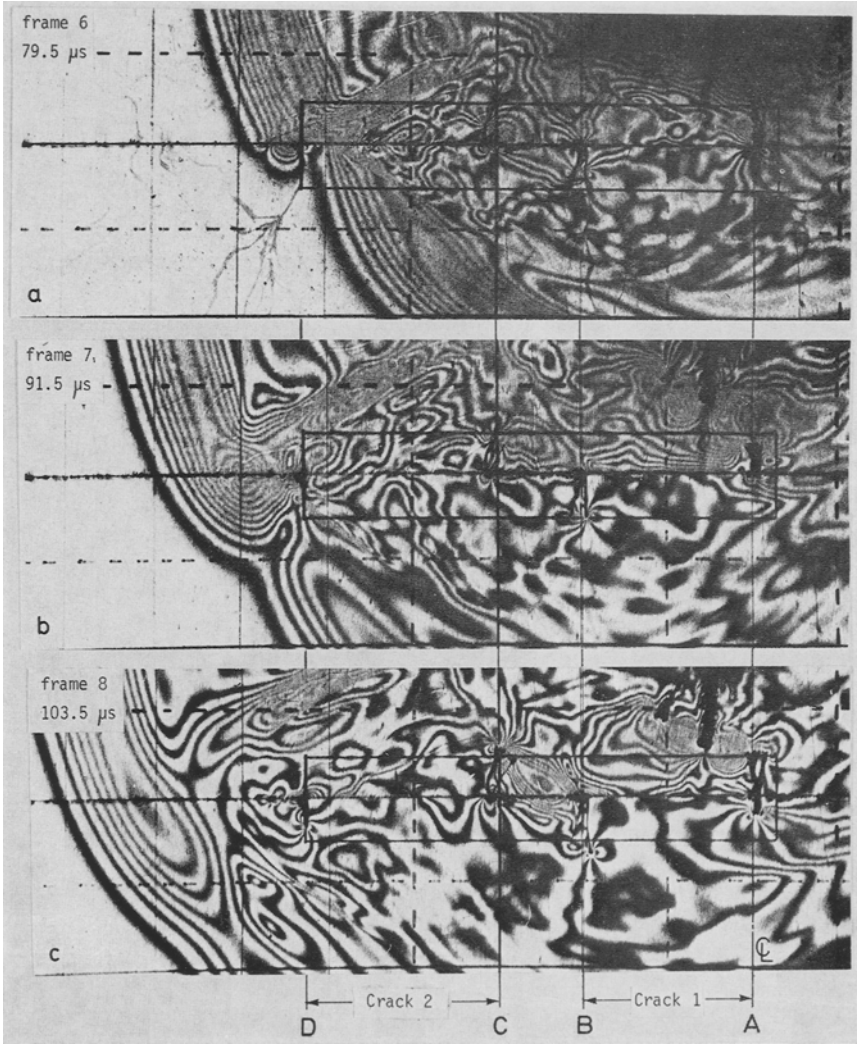

Fig. 9. Dynamic photoelastic recording of cylindrical stress wave (P, S) interaction with cracks situated at an imperfectly epoxy-resin bonded interface between two half-planes of Homalite 100 (Test LM-4)

symmetry of the wave problem and generates a shear wave with an unpredictable randomly circumferential amplitude distribution. Hence, the

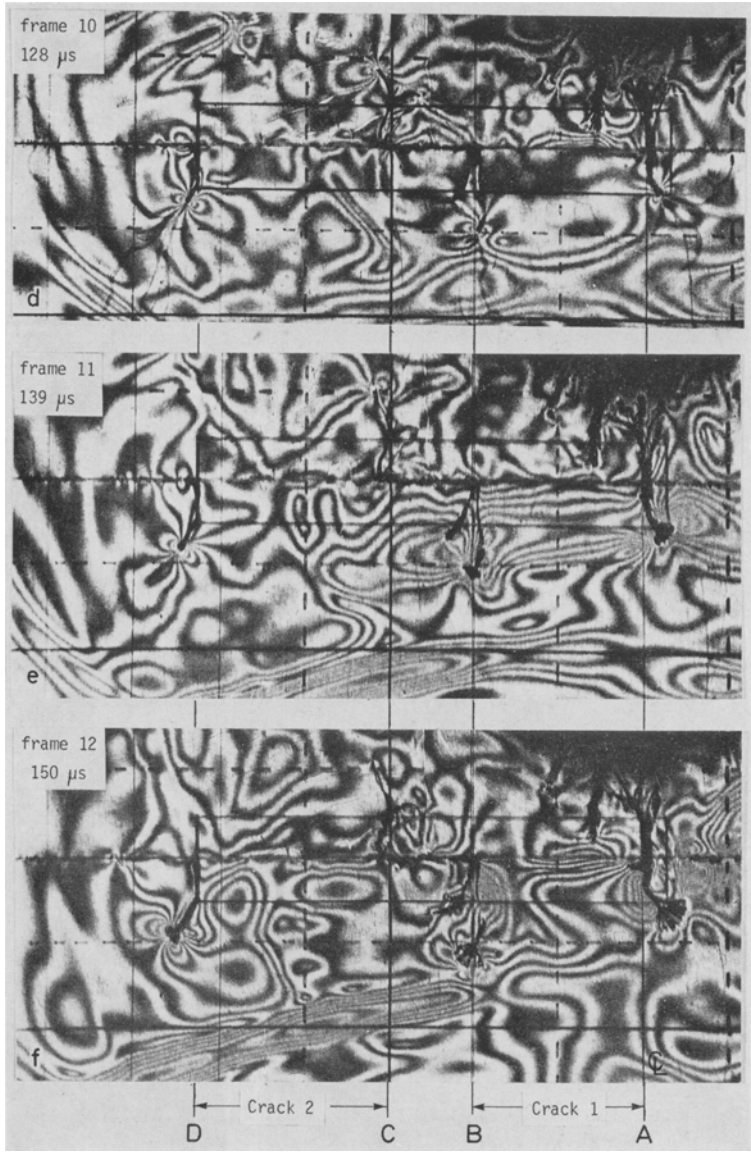

Fig. 9

Fig. 10. Sketch showing the orientation of unit normals to the crack tips

centerline marked C_L in the photographs does not imply zero-amplitude conditions for the shear wave as would be the case if the explosive had been detonated at a free boundary parallel to the interface line. As mentioned earlier, the interaction of the shear wave with crack tip A gives rise to a layer-crack which propagates from tip A downward away from the borehole layer (clearly visible in Fig. 9c).

The continuous flow of fringes across the bond sections $\overline{BC}$ bridging the two cracks in Fig. 9c indicates that this part of the interface has not been broken during the passage of the low amplitude trailing tensile part of the P-wave. Fig. 9c shows also the S-wave interaction with the P-wave generated layer branch cracks especially in the vicinity of crack tips B and C. Shear stress wave loading of static and/or moving cracks induces rapid changes of the instantaneous mixed-mode stress intensity factor resulting in crack path instability and promotes or delays crack branching in situations where the value of the nominal stress intensity factor is close to its critical value for crack branching [23]. Fig. 9d, frame 10, shows the fully developed branching pattern for the layer cracks emerging from tips A and C. Fig. 9c exhibits one more important feature. The continuous flow of isochromatic fringes of the leading compressive P-wave pulse across the bondline on the left of crack tip D, indicates perfect bonding with no additional imperfections present.

P-wave interaction with the free boundaries of the specimen gives rise to reflected P_rP and S_rP-waves which can clearly be distinguished in Fig. 9e by the isochromatics linking up the tips of the layer cracks from A and B. The reflected P_rP-wave has started to interact with cracks emerging from interface crack tips, A and B and is causing branching to occur. Because of its reflections at a free boundary of the model the leading part of the reflected P-wave causes a state of biaxial tension. Reorientation of the propagating cracks occurs due to the changing direction of principal tensile stress. Part of the energy carried by the reflected P-wave is transferred into crack driving energy. The cracks, however, are already propagating at terminal velocity and the cracks respond to any further supply of energy by branching. This is clearly visible from frames 11 and 12 in Figs. 9e and 9f. The high amplitude wave front in the lower part of Figs. 9e and 9f is the S_rP shear wave generated by P-wave reflection and its interaction with the already multiple-branched cracks causes more severe branching to occur.

Transmission of Waves and Cracks Across Interfaces

One of the most important aspects in dynamic fracturing is the transmission of waves and cracks across interfaces. The existence and the amplitude of reflected waves depends on the type and quality of the bonded area. Fig. 11 shows two illustrative examples of the transmission of obliquely incident longitudinal waves across bondlines in a jointed layered model. The central part of a nonhomogeneous P-wave front passes undisturbed across the near perfect bondline as shown in Fig. 11a. The presence of in-

clusions, micro cracks or debonded sites in the bond interface area can cause wave reflections and, hence, local *P*- and an *S*-wave disturbances can be generated at these sites along the interfaces. One of these very local reflected wave disturbances is indicated on the left hand side of Fig. 11a.

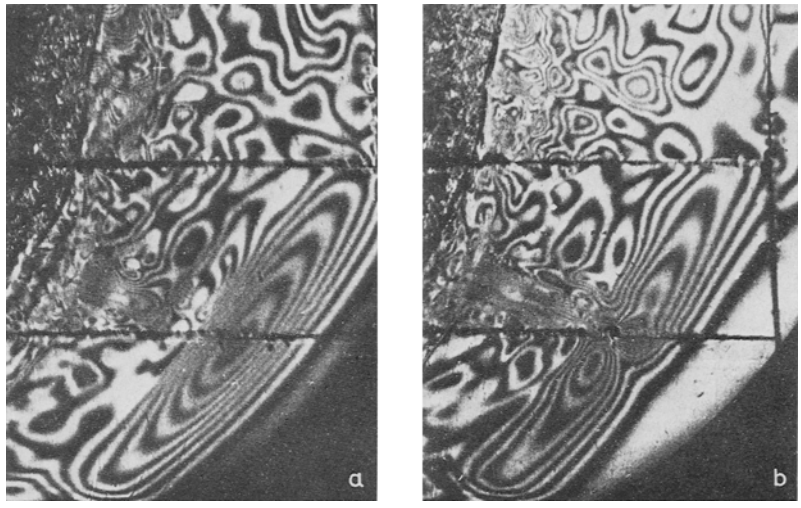

Fig. 11. Transmission of obliquely incident longitudinal waves across a (a) perfect bond and across an (b) imperfect bond in a jointed layered model showing reflected and transmitted waves

If the distribution of imperfections is more dense these local reflected wave disturbances connect and generate a continuous reflected wave front as shown in Fig. 11b. Notice that the central part of the *P*-wave is severely distorted. The reflected wave visible is the S_rP-wave. The amplitude of wave is much higher than the associated P_rP-wave which is not visible in the isochromatic fringe pattern distributions of Figs. 11a and 11b.

Cracks crossing an ideal bimaterial interface will be refracted at an angle that depends on the acoustic impedance mismatch of the two layers. For similar layers stacked and bonded together with a strong perfect bond of infinitesimal thickness no path deflection should occur during direct passage of the cracks. If, however, the adhesive bond is weaker than the adherend material secondary bond breakage ahead of the main crack can occur. Fig. 12 shows the indirect passage of a borehole crack across an imperfectly bonded joint. Stress concentrations developing along the bondline ahead of the main borehole crack (Fig. 12 a, b) cause shear fractures extending into both layers at an angle of about 45^0 (Fig. 12 b, c) and initiate progressive bond separation as shown in Figs. 12c and 12d. This is evident from the change in fringe order across the bondline. The main crack finally joins with the bondline separations to form a kinked crack which, although unfavorably oriented, continues to propagate along the interface. When

propagation along the interface becomes less favorable for the crack from an energy dissipative point of view, their branching of the crack from the interface into the layer material occurs in a direction forming the stretched Z-shaped crack path shown. Employing the concept of maximum dissipation rate of [28—29] the product of crack extension force $\mathfrak{G}$ times crack velocity c, $\mathfrak{G} \cdot c$ for incremental crack extension of the kinked crack (Fig. 12d),

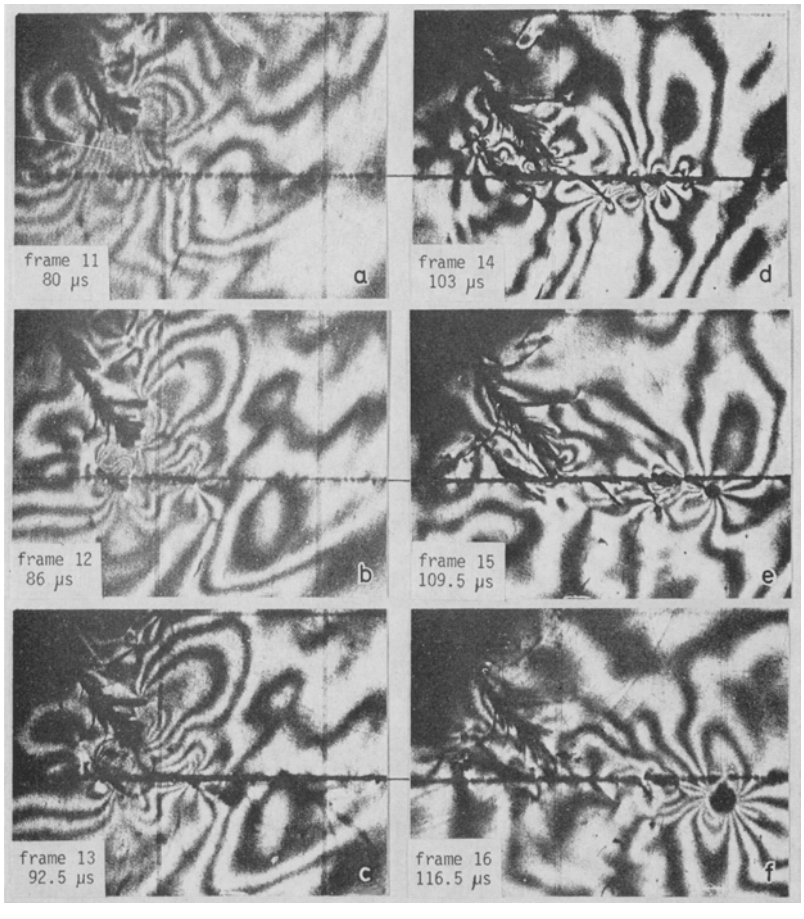

Fig. 12. Sequence of dynamic isochromatic fringe patterns showing the indirect passage of a borehole crack across an imperfectly bonded joint (Homalite 100 — Epoxy bond — Homalite 100) showing secondary bond breakage ahead of the main crack (Test LM-1, frames 11—16)

it is concluded that $(\mathfrak{G}_{c_L} \cdot c)_{\text{layer}} > (\mathfrak{G}_{c_B} \cdot c_B)_{\text{Bond}}$. Here, $\mathfrak{G}_{c_L}$ and $\mathfrak{G}_{c_B}$ are the strain energy release rates for the layer material and the bond, respectively, whereas c and $c\chi$ are the crack velocity in the layer material and the speed of debonding, respectively. Fig. 12f shows that the angle between the bondline and the two arms of the Z-crack are different.

Conclusions

Crack initiation from imperfections in interfaces between two homogeneous layers is a very complicated process. It has been observed that this initiation can occur either from the compressive peak of the outgoing *P*-wave or possibly from a combination of the tensile *P*-wave tail and the outgoing shear wave. Unlike initiations from joints with complete bonding, cracks initiate into the borehole layer and also layer adjoining the borehole. This process is further complicated by the possibility of load transmission due to crack closure or partial crack closure.

The experimental work described here as well reported earlier [30] has demonstrated the major role that larger flaws such as joints and bedding planes play in the fragmentation process. The initiation of these fractures at right angles to the joint sets helps to explain why fragmentation seen at a quarry site is rectangular in shape and why fragment size increases as the distance from the borehole increases.

This mechanism of fragmentation becomes even more complicated when the two adjoining layers are of different materials. A second paper describes experimental results obtained from tests in such models.

Acknowledgement

The authors were supported in this research program by DOE Contract No. DE-AP21-79MC-12577. Mr. Charles Komar was monitor of the contract. Part of the support for Dr. H. P. Rossmanith was provided from the Fonds zur Förderung der wissenschaftlichen Forschung in Austria under Project No. 3864. The authors would like to acknowledge Mr. J. P. Waskey who conducted the experiments and Ms. Judith Clark who typed the manuscript.

References

[1] Kolsky, H.: Stress Waves in Solids, Dover (1963).

[2] Ewing, W. M., Jardetzky, W. S., and Press, F.: Elastic Waves in Layered Media. New York: McGraw-Hill 1957.

[3] Achenbach, J. D.: Wave Propagation in Elastic Solids. Amsterdam: North Holland Co. 1973.

[4] Graff, K. F.: Wave Motion in Elastic Solids. Ohio State University Press. 1975.

[5] Miklowitz, J.: Elastic Wave Propagation, Applied Mechanics Surveys. New York: Spartan Books 1966.

[6] Cagniard, L.: Reflection and Refraction of Progressive Seismic Waves. New York: McGraw-Hill 1962.

[7] White, J. E.: Seismic Waves: Radiation, Transmission, and Activation. New York: McGraw-Hill 1965.

[8] Muskat, M., and Meres, M. W.: Reflection and Transmission Coefficients for Plane Waves in Elastic Media. Geophysics *5*, 149—155 (1940).

[9] Heelan, P. A.: On the Theory of Head Waves. Geophysics *18*, 871—893 (1953).

[10] Schmitt, A. B., and Bostick, F. X., Jr.: Propagation of Elastic Waves in Layered Media. Office of Naval Research, Washington, D. C., Report No. 142, 1966 (No. 375 (17), NR 081-253).

[11] Brekhovskikh, L. M.: Waves in Layered Media. Transl. by D. Lieberman, ed. by T. R. Beyer. New York: Academic Press 1960.

[12] Chen, P. E., and Sih, G. C.: Chapt. 1 and 3 in "Elastodynamic Crack Problems" in Mechanics of Fracture *4* (ed. by G. C. Sih), Leyden: Noordhoff Int. Publ. 1977.

[13] Brock, L. M.: The Stresses and Strain Energy Density Near a Crack Edge Due to *P*- and *SV*-Wave Diffraction. Developments in Mechanics, Vol. 8, Proc. 14th Midwestern Mech. Conf., 125—139 (1975).

[14] Nuismer, R. J., Jr., and Achenbach, J. D.: Dynamically Induced Fracture. J. Mech. Phys. Solids *20*, 203—222 (1972).

[15] Riley, W. F., and Dally, J. W.: A Photoelastic Analysis of Stress Wave Propagation in a Layered Model. Geophysics *31*, 881—889 (1966).

[16] Riley, W. F., and Dally, J. W.: Recording Dynamic Fringe Patterns with a Cranz-Schardin Camera. Exp. Mech. *9*, 37N—33N (1969).

[17] Daniel, I. M., and Marino, R. L.: Wave Propagation in a Layered Model Due to Point Source Loading in a High Impedance Medium. Geophysics *35*, 517—532 (1971).

[18] Burger, C. P., and Riley, W. F.: Effect of Impedance Mismatch on the Strength of Waves in Layered Solids. Exp. Mech. *14*, 129—137 (1974).

[19] Barker, D. B., Fourney, W. L., and Dally, J. W.: Photoelastic Investigation of Fragmentation Mechanisms. Part I — Borehole Crack Network. NSF-Report, University of Maryland, 1978.

[20] Barker, D. B., and Fourney, W. L.: Photoelastic Investigation of Fragmentation Mechanisms. Part II — Flaw Initiated Networks. NSF-Report, University of Maryland, 1978.

[21] Rossmanith, H. P.: Dynamic Fracture in Glass. NSF-Report, University of Maryland, 1978.

[22] Fourney, W. L., and Barker, D. B.: Effect of Time Delay on Fragmentation in a Jointed Model. NSF-Report, University of Maryland, 1979.

[23] Rossmanith, H. P., and Shukla, A.: Dynamic Photoelastic Investigation of Interaction of Stress Waves with Running Cracks. Proc. SESA Spring Meeting, Boston, 1980, Exp. Mech. *21* (II), 1981.

[24] Rossmanith, H. P.: Experimental Study of Diffraction of Elastic Waves About Stationary Interface Cracks. IUTAM-Conference, Toronto, 1980.

[25] Rossmanith, H. P., and Shukla, A.: Transient Mixed-mode Stress Intensity Factors During Elastic Wave Diffraction at Stationary and Moving Crack Tips. 14th U. S. Nat. Conf. Fract. Mechanics, Los Angeles, 1981 (to appear in ASTM-STP).

[26] Dally, J. W.: Data Analysis in Dynamic Photoelasticity. Exp. Mech. *7*, 1—7 (1967).

[27] Philips, J. W.: Private communication, 1979.

[28] Rossmanith, H. P., and G. R. Irwin: Analysis of Dynamic Isochromatic Crack-Tip Stress Patterns, Univ. of Maryland Report, July 1979.

[29] Rossmanith, H. P., and G. R. Irwin: Application of the Maximum Energy Dissipation Rate Principle to Crack Extension (submitted for publication).

[30] Fourney, W. L., Barker, D. B., and Holloway, D. C.: Explosive Fragmentation of a Jointed Brittle Media, submitted to Intern. Journ. of Rock Mech. and Mining Sciences.

Addresses of the authors: Doz. Dr. H. P. Rossmanith, Institut für Mechanik, Technische Universität Wien, Karlsplatz 13, A-1040 Wien, Austria; Prof. Dr. W. L. Fourney, Department of Mechanical Engineering, University of Maryland, College Park, MD 20742, U. S. A.